

Lattice Dynamics and Thermal Equation of State of Platinum

Tao Sun,¹ Koichiro Umemoto,² Zhongqing Wu,²

Jin-Cheng Zheng,³ and Renata M. Wentzcovitch^{2,*}

¹*Department of Physics and Astronomy,*

Stony Brook University, Stony Brook, New York 11794

²*Department of Chemical Engineering and Materials Science,*

Minnesota Supercomputing Institute,

University of Minnesota, Minneapolis, Minnesota 55455

³*Condensed Matter Physics & Materials Science Department,*

Brookhaven National Laboratory, Upton, New York 11973

(Dated: October 26, 2018)

Abstract

Platinum is widely used as a pressure calibration standard. However, the established thermal EOS has uncertainties, especially in the high P - T range. We use density functional theory to calculate the thermal equation of state of platinum, up to 550 GPa and 5000 K. The static lattice energy is computed by using the LAPW method, with LDA, PBE, and the recently proposed WC functional. The electronic thermal free energy is evaluated using the Mermin functional. The vibrational part is computed within the quasi-harmonic approximation using density functional perturbation theory and pseudopotentials. Special attention is paid to the influence of the electronic temperature to the phonon frequencies. We find that in overall LDA results agree best with the experiments. To provide accurate thermal EOS for pressure calibration, we combine the computed temperature dependence of the Gibbs energy with the room temperature Gibbs free energy corrected by experiments. The resulting thermal EOS seems reasonably accurate and we encourage its use as a reference for pressure calibration.

PACS numbers: 64.30.Ef, 05.70.Ce, 71.15.Mb, 63.20.D-

I. INTRODUCTION

Platinum (Pt) is a widely used high-pressure standard. Its equation of state (EOS) at room temperature has been established by reducing shock Hugoniot^{1,2,3,4} and by *ab initio* linear-muffin-tin-orbital (LMTO) calculations⁴ up to 660 GPa. Mao *et al.*⁵ used the EOS developed in Ref. 4 (Holmes *et al.*) to calibrate pressure in their compression experiments on Fe and Fe-Ni alloy. The bulk moduli measured at the earth's core pressure are substantially higher than those extrapolated from seismological observations.⁶ It is suspected that Holmes *et al.*'s EOS overestimates pressure, about 8% at 100 GPa, 15% at 300 GPa. Dewaele *et al.*⁷ measured the EOS of six metals at ambient temperature to 94 GPa using a diamond anvil cell (DAC). By cross-checking different pressure scales they found Holmes *et al.*'s EOS overestimates pressure by ≈ 4 GPa near 100 GPa at room temperature. This conclusion is confirmed by other groups.⁸

However, more recent calculations based on density functional theory (DFT) show a different picture. Xiang *et al.*⁹ compute the thermal equation of state of platinum using LMTO and a mean field potential method. Their isotherm at 300 K is even stiffer than that of Holmes *et al.*, indicating the latter underestimates, rather than overestimates, pressure. Menéndez-Proupin *et al.*¹⁰ reach similar conclusion using pseudopotentials. Both calculations employ the local density approximation (LDA) functional.¹¹ The excess pressure may originate in LDA, as suggested in Ref. 10. It can also be caused by other factors. In Table II of Ref. 9, the equilibrium volume decreases as the temperature increases. The electronic thermal pressure is negative according to this calculation, which is contrary to expectations. Ref. 10 uses an ultrasoft Rappe-Rabe-Kaxiras-Joannopoulos pseudopotential from the PWSCF website,¹² which contains only $5d$, $6s$ and $6p$ valence states. Its large cutoff radius (2.6 a.u.) may cause error in studying the highly compressed structure.

Besides the room temperature isotherm, accurate thermal pressure (P_{th}) is needed to calibrate pressure in simultaneous high-pressure and high-temperature experiments. Experiments cannot easily determine P_{th} over a wide temperature and volume range.¹³ Consequently P_{th} is often estimated by assuming it is linear in temperature and independent of volume.^{1,4} Theory can in principle do better. In quasi-harmonic approximation (QHA), DFT calculations give P_{th} at any particular temperature and volume, and reveal many qualitative features. It is desirable to find ways to improve the accuracy of the DFT results so that

they can serve as credible references for pressure calibration.

In this paper we have three goals: first is to check the accuracy of the theoretical EOS of platinum predicted by different exchange correlation functionals. In contrast with previous calculations, we find the room temperature isotherm computed with LDA lies below, and nearly parallel to the experimental compression data. The Fermi level of platinum lies in the d band and gives a very large density of state (DOS) $N(E_F)$. Its vibrational frequencies are more sensitive to the electronic temperature than those of many other metals. A Kohn anomaly has been observed in platinum at 90 K.¹⁴ It becomes weaker and finally disappears when the temperature increases. Thus our second goal is to discuss the {electronic temperature dependence of vibrations} (ETDV) and its influence on the thermal properties. Our last goal is to provide an accurate thermal EOS for pressure calibration. For this purpose we make corrections to the raw DFT results. We correct the room temperature Gibbs free energy $G(P, 300 \text{ K})$ to ensure that it reproduces the experimental isotherm, then combine it with the DFT calculated temperature dependence to get $G(P, T)$. The thermal EOS and thermal properties deduced from the corrected Gibbs free energy are in good agreement with the known experimental data.

II. COMPUTATIONAL METHOD

The EOS of a material is determined by its Helmholtz free energy $F(V, T)$, which consists of three parts:

$$F(V, T) = U(V) + F_{\text{vib}}(V, T) + F_{\text{ele}}(V, T), \quad (1)$$

where $U(V)$ is the static energy of the lattice, $F_{\text{vib}}(V, T)$ is the vibrational free energy, $F_{\text{ele}}(V, T)$ accounts for the thermal excitation of the electrons. $U(V)$ is calculated by using the linearized augmented plane-wave (LAPW) method¹⁵ and three different exchange-correlation functionals: LDA, Perdew-Burke-Ernzerhof (PBE),¹⁶ and Wu-Cohen (WC).¹⁷ The $4f$, $5s$, $5p$, $5d$, $6s$ are described as valence states, others are treated as core states. The convergence parameter RK_{max} is 10.0, and the muffin-tin radius R is 2.08 a.u.. A $16 \times 16 \times 16$ Monkhorst-Pack¹⁸ uniform k-grid is used and the integration over the whole Brillouin zone is done with the tetrahedron method.¹⁹ All the calculations using LAPW are performed with and without spin-orbit effect.

In contrast with the static lattice energy $U(V)$, which is sensitive to the relaxation of the

core states and requires a full-potential treatment, thermal excitations contribute to much smaller energy variations and mostly depend on the valence states. We use pseudopotentials to compute the thermal effects. An ultra-soft Vanderbilt pseudopotential²⁰ is generated from the reference atomic configuration $5s^25p^65d^96s^16p^0$, including non-linear core corrections.²¹ There are two projectors in the s channel, $5s$ and $6s$; two in the p channel, $5p$ and an unbound p at 0.2 Ry above the vacuum level; one in the d channel, $5d$. The local component is set in the f channel at the vacuum level. The cutoff radii for each channel s , p , d and local are 1.8, 1.9, 1.9, 1.8 a.u. respectively. We use the scalar relativistic approximation and spin-orbit effect is not included. This pseudopotential reproduces the LAPW electronic band structure, both at the most contracted volume and the 0 GPa experimental volume. We find pseudopotentials with different exchange-correlation functionals yield very similar electronic band structures for platinum, and we use LDA to compute all the thermal effects.

We consider 20 different volumes, with lattice constants from 7.8 to 6.2 a.u. (17.58 Å³ to 8.83 Å³ in volume). For each volume V_i , we use LAPW to compute its static energy $U(V_i)$ and the LDA pseudopotential to evaluate its thermal free energy $F_{\text{vib}}(V_i, T)$ and $F_{\text{ele}}(V_i, T)$. $F_{\text{vib}}(V_i, T)$ is treated within QHA with phonon frequencies dependent on electronic temperature (denoted as eQHA) as

$$F_{\text{vib}}^{\text{eQHA}}(V_i, T) = \frac{1}{2} \sum_{\mathbf{q}, j} \hbar \omega_{\mathbf{q}, j}(V_i, T_{\text{ele}}) + k_B T \sum_{\mathbf{q}, j} \ln(1 - \exp(\frac{-\hbar \omega_{\mathbf{q}, j}(V_i, T_{\text{ele}})}{k_B T})), \quad (2)$$

where $\omega_{\mathbf{q}, j}(V_i, T_{\text{ele}})$ denotes the phonon frequency computed at volume V_i and electronic temperature T_{ele} . In thermal equilibrium the system temperature T , the ionic temperature T_{ion} , and T_{ele} are equal. We distinguish these three temperatures to emphasis the temperature dependence of phonon frequencies come from different sources. Anharmonic phonon-phonon interactions cause phonon frequencies to depend on T_{ion} , but they are omitted in QHA. Electronic thermal excitations disturb the charge distribution in the crystal and cause phonon frequencies depend on T_{ele} . In the normal QHA used for insulators and some metals, this effect is also ignored and $\omega_{\mathbf{q}, j}$ has no temperature dependence (except through $V(T)$). Platinum has a larger $N(E_F)$ than many other metals and ETDV may have noticeable effects on its thermal properties. To quantitatively measure the influence of ETDV, we compare the vibrational free energies at volume V_i and temperature T_j ($T_j=500, 1000, \dots 5000$ K) computed without/with ETDV. Without ETDV (normal QHA), phonon frequencies are computed at $T_{\text{ele}}=0$ K by using Methfessel-Paxton²² (MP) smearing with

a smearing parameter of 0.01 Ry. The corresponding vibrational free energy is denoted as $F_{\text{vib}}^{\text{QHA}}(V_i, T_j)$. With ETDV (eQHA) phonon frequencies have to be computed separately for each T_j . This is achieved by using the Mermin functional²³ and Fermi-Dirac (FD) smearing. The corresponding vibrational free energy is denoted as $F_{\text{vib}}^{\text{eQHA}}(V_i, T_j)$. The difference between these two, $\Delta F_{\text{ETDV}}(V_i, T_j) = F_{\text{vib}}^{\text{eQHA}}(V_i, T_j) - F_{\text{vib}}^{\text{QHA}}(V_i, T_j)$, describes the correction caused by ETDV. To get ΔF_{ETDV} at arbitrary temperature between 0-5000 K we fit a 4th order polynomial from $\Delta F_{\text{ETDV}}(V_i, T_j)$

$$\begin{aligned}\Delta F_{\text{ETDV}}(V_i, T) &= F_{\text{vib}}^{\text{eQHA}}(V_i, T) - F_{\text{vib}}^{\text{QHA}}(V_i, T) \\ &= a_1(V_i) \cdot T + a_2(V_i) \cdot T^2 + a_3(V_i) \cdot T^3 + a_4(V_i) \cdot T^4.\end{aligned}\quad (3)$$

The final vibrational free energy is computed as $F_{\text{vib}}(V_i, T) = F_{\text{vib}}^{\text{QHA}}(V_i, T) + \Delta F_{\text{ETDV}}(V_i, T)$ (we omit the subscript ‘eQHA’ and denote $F_{\text{vib}}^{\text{eQHA}}$ as F_{vib}).

Phonon frequencies in the above procedure are determined by density functional perturbation theory (DFPT)²⁴ as implemented in the Quantum ESPRESSO²⁵ package. The dynamical matrices are computed on an $8 \times 8 \times 8$ \mathbf{q} -mesh (29 \mathbf{q} points in the irreducible wedge of the Brillouin Zone). Force constant interpolation is used to calculate phonon frequencies at arbitrary \mathbf{q} vectors. The summation in Eq. (2) is evaluated on a $32 \times 32 \times 32$ \mathbf{q} -mesh.

The electronic free energy $F_{\text{ele}}(V_i, T)$ is determined by using the Mermin functional²³ and Fermi-Dirac smearing. Similar to getting $F_{\text{vib}}(V_i, T)$, we first compute F_{ele} at every 50 K from 50 K to 5000 K, then we fit them to a 4th order polynomial

$$F_{\text{ele}}(V_i, T) = b_1(V_i) \cdot T + b_2(V_i) \cdot T^2 + b_3(V_i) \cdot T^3 + b_4(V_i) \cdot T^4.\quad (4)$$

Terms other than $b_2(V_i)T^2$ represent deviations from the lowest-order Sommerfeld expansion $F_{\text{ele}} = -\frac{\pi^2}{6}N(E_F)(k_B T)^2$. We combine $F_{\text{ele}}(V_i, T)$ with the static energy $U(V_i)$ from LAPW and the vibrational free energy $F_{\text{vib}}(V_i, T)$ from the same pseudopotential to get the total free energy $F(V_i, T)$ at volume V_i . There are two popular parameterized forms to fit the total free energy $F(V, T)$, 4th order Birch-Murnahan²⁶(BM) and Vinet.²⁷ We find BM and Vinet are comparable in accuracy to fit the static and low temperature free energy, but BM yields much lower residual energies than Vinet for the high temperature results. Thus we use 4th order BM to get $F(V, T)$, although for static and room temperature EOS the Vinet forms are also given. Other thermodynamical properties are computed by finite difference.

All the pseudopotential calculations are carried out with the same plane-wave cutoff of 40 Ry, charge-density cutoff of 480 Ry, and a shifted $16 \times 16 \times 16$ Monkhorst-Pack mesh. Extensive tests are carried out to ensure all the quantities of interest are well-converged.

III. SUMMARY OF PREVIOUS WORKS

Besides the two calculations^{9,10} mentioned in the introduction, which focus on the thermal EOS of platinum, there are some other papers related to this subject. Cohen *et al.*²⁸ computed the static EOS of platinum using LAPW and PBE, and treated it as an example to discuss the accuracy of different EOS formations. They found Vinet fitted better than 3rd order BM. The accuracy of 4th order BM and Vinet were comparable. Tsuchiya *et al.*²⁹ computed the electronic thermal pressure (P_{ele}) of Au and Pt using LMTO and LDA. At 2200 K, P_{ele} is 1.01 GPa for Pt, while only 0.06 GPa for Au. This is caused by the different $N(E_F)$ of the two metals. Wang *et al.*³⁰ used LAPW and an average potential method to determine the thermal contributions. Then they reduced the experimental shock Hugoniot and got the room temperature isotherm of Pt. This isotherm is very similar to that of Holmes *et al.*, in spite of the fact that in the latter case, thermal pressure is estimated semi-empirically. Ref. 31 computed the static EOS of platinum using pseudopotentials with/without spin-orbit effects up to 150 GPa. Recently, Dorogokupets *et al.*³² constructed a complicated semi-empirical model to describe the thermal properties of Al, Au, Cu, Pt, Ta and W. This model contains about 20 parameters, which are fitted to the available experimental data on the heat capacity, enthalpy, volume, thermal expansivity, bulk modulus and shock Hugoniot. The advantage of such an approach is all the thermal properties are treated as a whole and it is easier to achieve internal consistency. However, if some of the experimental data are less accurate, they may affect the accuracy of the whole model. Using simplified analytical forms to describe the complicated thermal behavior of the real materials may also introduce uncertainties. In the following section, we compare our calculations with these previous ones whenever appropriate.

On the experimental side, The shock Hugoniot reported in Ref. 1 was obtained by using chemical explosives. The reduced room temperature isotherm was up to 270 GPa. Holmes *et al.*⁴ went to higher compression ratio using a two-stage light-gas gun. The final shock Hugoniot is a combination of these two sets of data. A. D. Chijioke³³ *et al.* discussed that

neglecting the shear strength of the material causes error in reducing the shock Hugoniot. The high-pressure melting curve of platinum is measured by Kavner *et al.* up to 70 GPa.³⁴ With the development of DAC and third-generation synchrotron light source, cross-checking different pressure scales becomes feasible. More accurate thermal EOS are obtained by using this method.^{7,13}

IV. RESULTS AND DISCUSSIONS

A. Static Equation of State

Before studying the EOS at finite temperature, we examine the static EOS computed by using different exchange-correlation functionals, and compare them with previous calculations. Excluding the thermal effects (which amount to ≈ 2 GPa at room temperature) helps to identify the origin of their differences. Fig. 1 shows the static pressure vs. volume relations using different exchange-correlation functionals. The corresponding EOS parameters are listed in Table I. The experimental data at room temperature are also included in the figure to give a rough estimate of the difference. Comparing to the experiments, in the entire volume range LDA underestimates pressure while PBE overestimates. WC improves on PBE, but still overestimates. A detailed comparison between the calculated room temperature isotherms (including the thermal effects) and the experimental data will be given in Sec. IV C. DFT has many different implementations, such as LAPW, LMTO, and various pseudopotentials. If the calculations are good, they should yield similar results. We compare our LDA calculations with previous ones in Fig. 2. Two of our own pseudopotential calculations are included for comparison. One is the Vanderbilt pseudopotential that we used to compute the thermal effects, denoted as pseudo-1. The other is a Rappe-Rabe-Kaxiras-Joannopoulos pseudopotential from the PWSCF website (Pt.pz-nd-rrkjus.UPF), denoted as pseudo-2. The static EOS predicted by pseudo-1 is similar to that of LAPW, except in the high pressure range, where the relaxation of the core electrons becomes prominent. The previous overestimations of pressure are probably caused by the large cutoff radius (Ref. 10) or another issue related to the negative electronic thermal pressure (Ref. 9).

Platinum is a heavy element, and its electronic band structure is sensitive to spin-orbit effect.³⁶ We find inclusion of the spin-orbit effect increases the equilibrium volume, no matter

TABLE I: Static EOS parameters obtained from LAPW calculations and compared those in literature. Parameters from the pseudopotential calculations (pseudo-1 and 2) are also listed. For convenience both Vinet and 4th order BM parameters are shown. V_0 denotes the equilibrium volume, K_0 , K'_0 and K''_0 are the isothermal bulk modulus, the first and second derivative of the bulk modulus at V_0 , respectively. Note their different fitting ranges: 0-550 GPa (this study), 0-1000 GPa (Ref. 9), 0-660 GPa (Ref. 10), 0-150 GPa (Ref. 31), 0-350 GPa (Ref. 28). Ref. 31 uses 3rd order BM EOS so the corresponding K''_0 are not listed.

| | Vinet | | | B-M | | | |
|----------------------------|--------------------------|-------------|--------|--------------------------|-------------|--------|-------------------------------|
| | V_0 (\AA^3) | K_0 (GPa) | K'_0 | V_0 (\AA^3) | K_0 (GPa) | K'_0 | K''_0 (GPa^{-1}) |
| LDA | 14.752 | 308.02 | 5.446 | 14.761 | 309.29 | 5.295 | -0.02666 |
| LDA+SO | 14.784 | 301.17 | 5.533 | 14.785 | 301.13 | 5.510 | -0.03214 |
| LDA(pseudo-1) | 14.719 | 308.69 | 5.423 | 14.726 | 309.61 | 5.295 | -0.02681 |
| LDA(pseudo-2) | 15.055 | 297.48 | 5.515 | 15.060 | 299.28 | 5.375 | -0.02873 |
| LDA ^a | 14.90 | 300.9 | 5.814 | | | | |
| LDA ^b | 15.073 | 293 | 5.56 | | | | |
| LDA ^c (HGH) | | | | 14.82 | 305.99 | 5.32 | — |
| LDA+SO ^{c,d} (TM) | | | | 15.2 | 291.18 | 5.35 | — |
| PBE | 15.679 | 242.50 | 5.639 | 15.678 | 245.88 | 5.464 | -0.03620 |
| PBE+SO | 15.751 | 231.97 | 5.762 | 15.754 | 229.96 | 5.850 | -0.04932 |
| PBE ^a | 15.77 | 243.3 | 5.866 | | | | |
| PBE ^c (HGH) | | | | 15.59 | 250.85 | 5.65 | — |
| PBE ^e | 15.69 | 248.9 | 5.43 | | | | |
| WC | 15.171 | 280.63 | 5.500 | 15.177 | 283.49 | 5.306 | -0.02889 |
| WC+SO | 15.223 | 269.97 | 5.630 | 15.223 | 269.00 | 5.670 | -0.03893 |

^aReference 9.

^bReference 10.

^cReference 31.

^dReference 35.

^eReference 28.

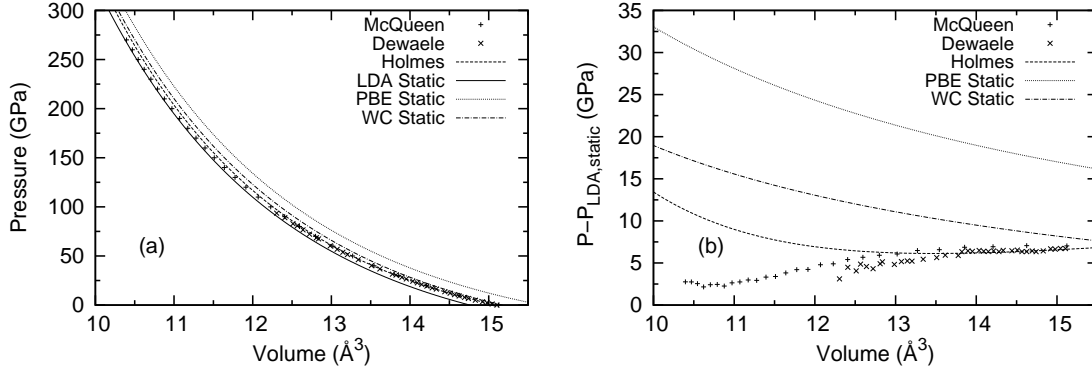


FIG. 1: Static EOS computed by the LAPW method using various exchange correlation functionals. (a). Pressure vs. volume curves, (b). Pressure difference with respect to the static LDA EOS. Experimental data labeled as ‘McQueen’ are from Ref. 1, ‘Dewaele’ from Ref. 7, ‘Holmes’ from Ref. 4.

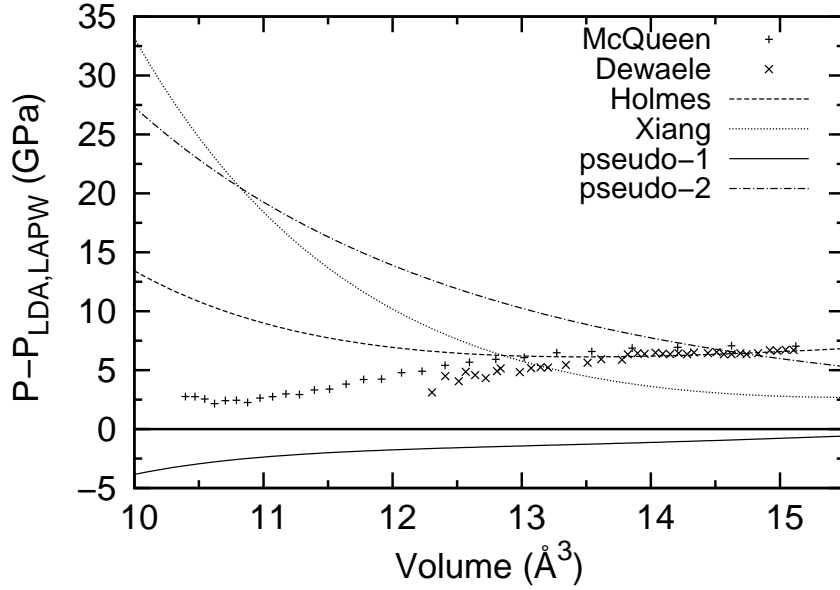


FIG. 2: Different LDA static EOS compared with the one computed by using LAPW. ‘Xiang’ denoted the EOS from Ref. 9.

which exchange correlation functional is used. This tendency has also been observed by Bercegeay *et al.*³¹ in their pseudopotential calculations. However, the EOS parameters are not independent of each other. The variation of the equilibrium volume largely compensates that of the bulk modulus and the actual pressure difference is less than 1 GPa when P is

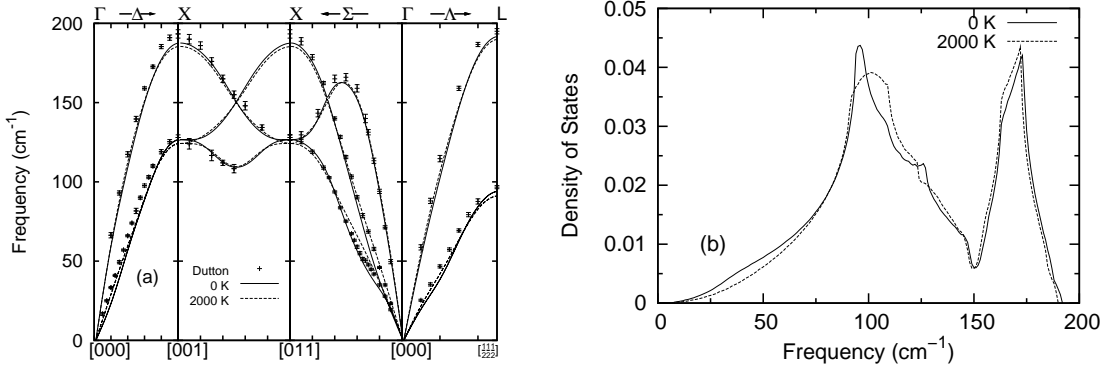


FIG. 3: (a) Phonon dispersion and (b) vibrational DOS at $a=7.4136$ a.u.. Solid line corresponds to $T_{\text{ele}}=0$ K, dashed line corresponds to $T_{\text{ele}}=2000$ K. They are calculated by using the LDA pseudopotential. Experimental data labeled as ‘Dutton’ are from Ref. 14.

below 250 GPa . Thus we conclude the spin-orbit effect is not very important in determining the EOS of platinum.

B. Phonon Dispersion and Its Electronic Temperature Dependence

Fig. 3 shows the phonon dispersions at the experimental ambient condition lattice constant $a=7.4136$ a.u..⁷ One is computed at $T_{\text{ele}}=0$ K. The other at $T_{\text{ele}}=2000$ K, close to platinum’s melting point at ambient pressure 2041.3 K.³⁴ The Kohn anomaly (near $\mathbf{q}=[0, 0.35, 0.35]$) disappears when the electronic temperature is high, and the vibrational DOS varies noticeably. The corresponding corrections to the vibrational free energy, $\Delta F_{\text{ETDV}}(V_i, T)$, are shown in Fig. 4 (a). ΔF_{ETDV} is always positive. As volume decreases, it diminishes and finally becomes negligible. ETDV originates in the thermal excitations of the electrons near the Fermi surface, and the number of thermal excited electrons is proportional to $N(E_F)$ in the lowest-order Sommerfeld expansion. For smaller volumes, the electronic bands are more dispersive and $N(E_F)$ decreases, as shown in Fig. 4(b). ETDV diminishes accordingly.

Figure 5 and 6 shows the volume thermal expansion coefficient α , heat capacity at constant pressure C_P , entropy S , and the temperature-dependent part of the Gibbs free energy $\Delta G(P, T)=G(P, T)-G(P, T = 300\text{K})$. Including ETDV improves agreement for all these properties. The remaining differences between theory and experiment are attributed to

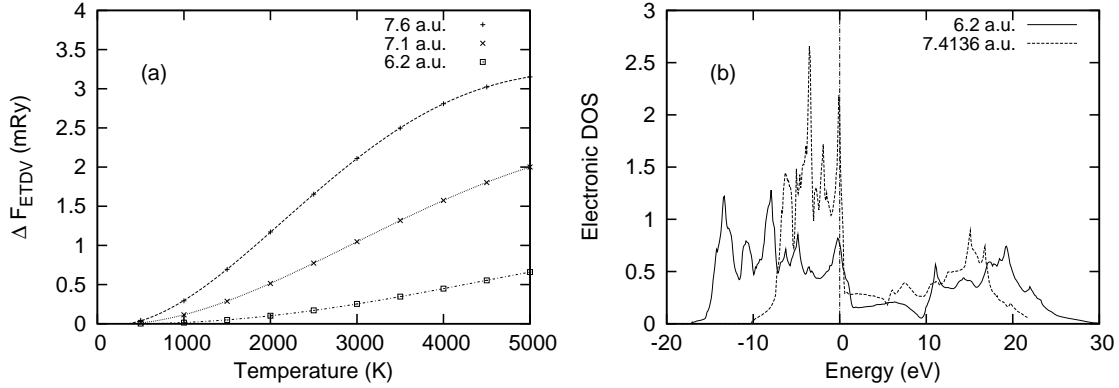


FIG. 4: (a) Corrections to the vibrational free-energy at various lattice constants. (b) Volume dependence of the electronic density of states.

anharmonic phonon-phonon interactions and electron-phonon interactions, which are not included in our treatment. Such omissions seem justifiable, since the remaining differences are relatively small. We compare the contributions to the thermal properties from ETDV (ΔF_{ETDV}) with those from pure electronic thermal excitations (F_{ele}). Although pure electronic thermal excitations have much larger influence on $\Delta G(P, T)$ than ETDV, as shown in Fig. 6(c). Their contributions to α , C_P (second derivatives of the free energy) are comparable, as shown in Fig. 5(a) and Fig. 6(a).

C. Room Temperature Isotherms

By fitting the total Helmholtz free energy at 300 K, we get the theoretical 300 K isotherms, as shown in Fig. 7. Their parameters are listed in Table II. In the low pressure range, the LDA isotherm and the experimental data are almost parallel. As pressure increases, they start to converge. It seems LDA works better at high pressures. Regarding to EOS parameters, LDA and WC give equilibrium volumes closest to the experiments, WC without spin-orbit effect yields closest bulk modulus (K_0) and the derivative of the bulk modulus (K'_0). Some people^{7,31} prefer to compare pressures from two EOS (labeled as EOS-I and EOS-II) at the same compression, i.e. the same value of V/V_0 . V_0 is the corresponding equilibrium volume, $V_{0,\text{I}}$ for EOS-I, $V_{0,\text{II}}$ for EOS-II. Such comparisons can give favorable agreement when K_0 and K'_0 of EOS-I are close to those of EOS-II, even $V_{0,\text{I}}$ and $V_{0,\text{II}}$ are quite different.⁷ As mentioned before, the EOS parameters are not independent of each

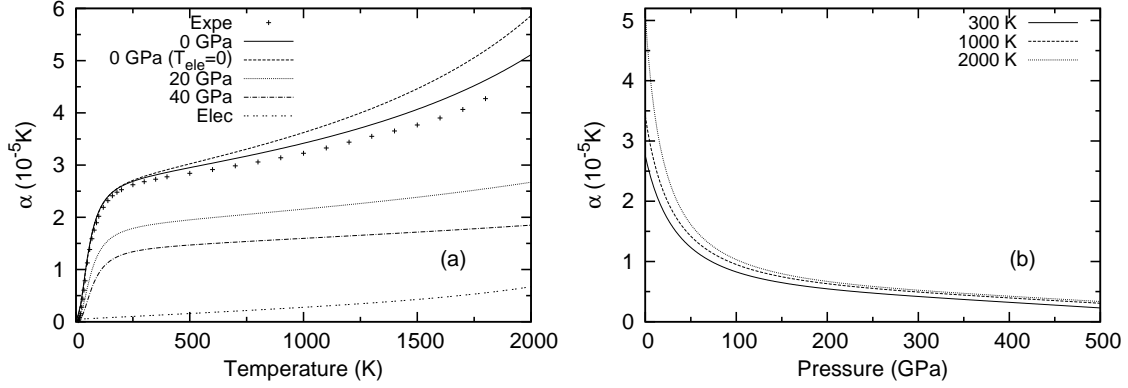


FIG. 5: Thermal expansivity as a function of (a) temperature and (b) pressure. Curves with label ‘(T_{ele}=0)’ represent properties computed without ETDV, i.e. computed from $F_{\text{vib}}^{\text{QHA}}$. Curves without this specification are the default ones computed with ETDV. ‘Elec’ is an exception. It corresponds to the contribution from pure electronic thermal excitations, which is the difference between the thermal properties calculated with/without the electronic thermal free energy F_{ele} . The experimental data are from Ref. 37.

other. Taking WC with/without spin-orbit effect as a example, their pressure vs. volume curves differ by less than 1 GPa in most regions, the difference between their pressure vs. compression curves is much larger. It can be fortuitous that K_0 and K'_0 agree well. We still prefer LDA as the optimal functional for platinum. It is worth noting the LDA (HGH) pressure vs. volume relation reported in Ref. 31 is similar to those obtained in this study. However, Ref. 31 presents data in volume vs. compression, and concludes LDA overestimates pressure by 8 GPa near 100 GPa. In fact, although $K_{0,\text{LDA}}$ (291 GPa from this study) is much larger than $K_{0,\text{expe}}$ (273.6 GPa from Ref. 7), the bulk modulus computed at the experimental equilibrium volume $V_{0,\text{expe}}$ (15.095 Å³) is 270 GPa, quite close to $K_{0,\text{expe}}$. Thus when plotted in pressure vs. volume, the isotherm computed by LDA is nearly parallel with the experimental data in the low pressure range.

D. Thermal EOS of Platinum for Pressure Calibration

It is quite a challenge to get an *ab initio* EOS with accuracy comparable to experiments at low pressures. Suppose the theoretical equilibrium volume $V_{0,\text{theo}}$ differs from $V_{0,\text{expe}}$ by 0.5%. This will cause a pressure difference of $K_0 \cdot \frac{\Delta V}{V} = 1.3$ GPa for platinum. Recently there

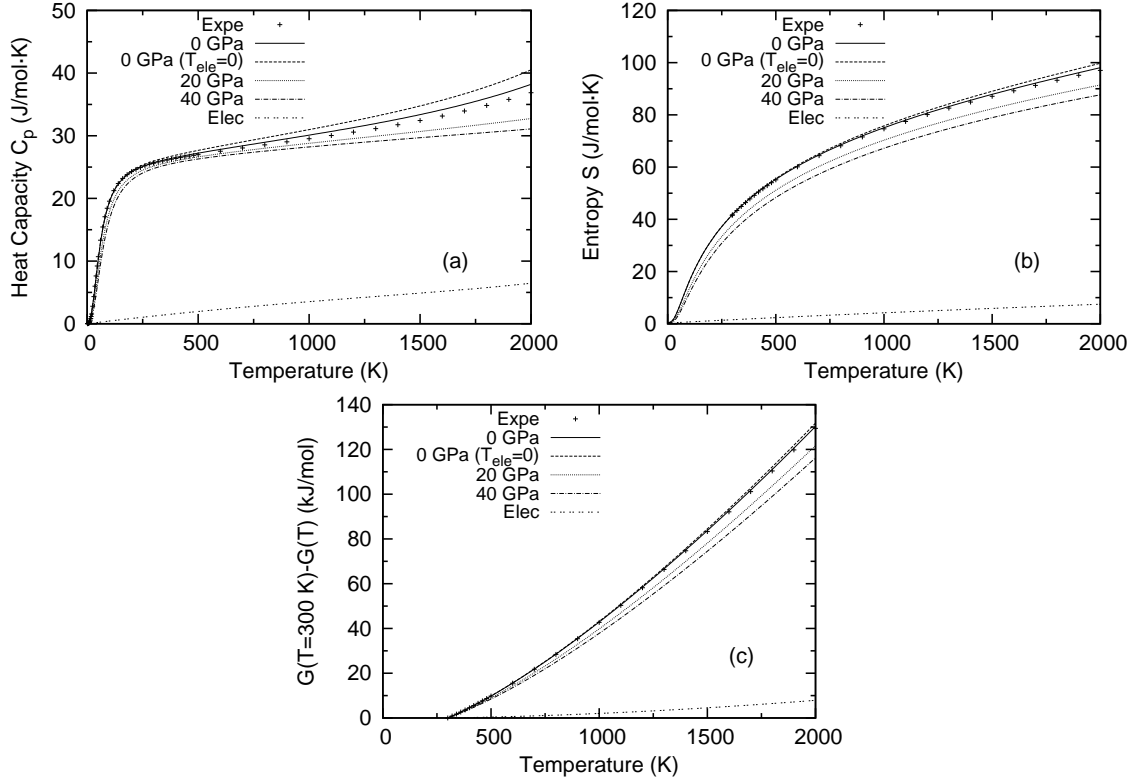


FIG. 6: Thermal properties of platinum. (a) Heat Capacity at constant pressure, (b) Entropy, (c) Temperature dependence of the Gibbs free energy at constant pressure. The meanings of the labels are the same as above. The experimental data are from Ref. 38.

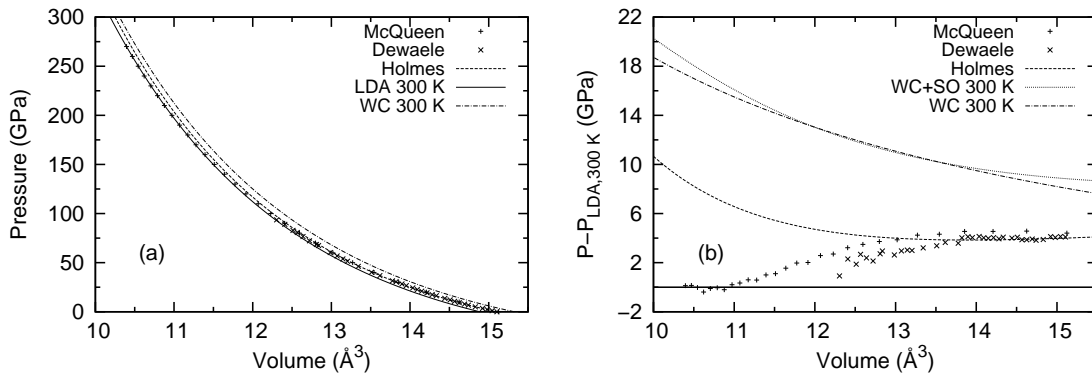


FIG. 7: 300 K isotherms. (a) pressure vs. volume. The correction caused by spin-orbit effect is too small to be identified in this scale (b) pressure difference. WC with spin-orbit effect is included. The difference between LDA and LDA+SO is of similar magnitude. PBE and PBE+SO are not plotted as their EOS are way off.

TABLE II: EOS parameters of the theoretical 300 K isotherms, compared with the experiments. $V_{0,\text{expe}}$ is 15.095 Å³. Pressure range: 0-550 GPa (this study), 0-660 GPa (Ref. 4 and 10), 0-94 GPa (Ref. 7), 0-270 GPa (Ref. 1).

| | Vinet | | | B-M | | | |
|-----------------------------|-------------------------|-------------|--------|-------------------------|-------------|--------|------------------------------|
| | V_0 (Å ³) | K_0 (GPa) | K'_0 | V_0 (Å ³) | K_0 (GPa) | K'_0 | K''_0 (GPa ⁻¹) |
| LDA | 14.884 | 291.25 | 5.547 | 14.886 | 291.65 | 5.496 | -0.03232 |
| LDA ($V_{0,\text{expe}}$) | | 269.96 | 5.640 | | 269.91 | 5.626 | -0.03730 |
| LDA+SO | 14.919 | 284.41 | 5.632 | 14.915 | 282.86 | 5.733 | -0.03909 |
| LDA ^a | 15.188 | 281 | 5.61 | | | | |
| PBE | 15.864 | 225.55 | 5.751 | 15.866 | 225.34 | 5.741 | -0.04709 |
| PBE+SO | 15.947 | 214.73 | 5.879 | 15.959 | 208.03 | 6.193 | -0.06571 |
| WC | 15.322 | 263.93 | 5.601 | 15.325 | 264.72 | 5.530 | -0.03580 |
| WC+SO | 15.381 | 252.98 | 5.737 | 15.381 | 249.08 | 5.940 | -0.04907 |
| Holmes ^b | 15.10 | 266 | 5.81 | | | | |
| Dewaele ^c | 15.095 | 273.6 | 5.23 | | | | |
| McQueen ^d | | | | 15.123 | 277.715 | 4.821 | -0.01379 |

^aReference 10.

^bReference 4.

^cReference 7. When K_0 is set to 277 GPa, the value measured by ultrasonic experiments, K'_0 equals 5.08 GPa.

^dReference 1, Fitted from the tabulated shock reduced isotherm at 293 K.

are attempts to use Quantum Monte Carlo (QMC) to get a more accurate EOS.³⁹ QMC avoids the approximations inherent in the exchange-correlation functionals, and should be more accurate. However, it is a very heavy calculation and other issues of accuracy become relevant, such as the size of the simulation cell. More tests are needed to see if QMC can meet the stringent accuracy requirements for pressure calibration.

There are attempts to combine the experimental data with DFT calculations to get a more accurate thermal EOS.^{30,40} The basic idea is to compute the thermal contributions, which are hard to determine experimentally, from DFT. Then, either add these contributions to the experimental room temperature isotherm (Ref. 40), or subtract them from the experimental

shock Hugoniot (Ref. 30). Here we follow the same spirit, although the details are different.

It is worthwhile to give a summary of our raw DFT results at this stage. We have computed the static lattice energy $U(V)$ using LAPW, and found spin-orbit interactions are not important in determining the EOS of platinum. We have used QHA to calculate the vibrational free energy $F_{\text{vib}}(V, T)$, and found including ETDV improves the agreement on the thermal properties. We have calculated the electronic free energy $F_{\text{ele}}(V, T)$ using Mermin functional. The resulting thermal properties, e.g. the temperature-dependent part of the Gibbs energy $\Delta G(P, T)$, are fairly accurate, in spite of the fact that our treatment does not include anharmonic phonon-phonon interactions and electron-phonon interactions. The room temperature isotherm computed by LDA merges to the experimental data at high pressures. The discrepancy in the low pressure range is what we hope to solve by introducing corrections.

We compare Dewaele's EOS⁷ ($V_0=15.095 \text{ \AA}^3$, $K_0=273.6 \text{ GPa}$, $K'_0=5.23$ in Vinet form) with our room temperature isotherm computed by LDA, without spin-orbit effect ($V_0=14.884 \text{ \AA}^3$, $K_0=291.25 \text{ GPa}$, $K'_0=5.547$ in Vinet form). The volume difference between these two at each pressure $\Delta V(P) = V_{\text{expe}, 300 \text{ K}}(P) - V_{\text{LDA}, 300 \text{ K}}(P)$ is shown in Fig. 8. Since $\Delta V(P)$ decreases rapidly as pressure increases, we use exponentially decaying functions for extrapolation. We correct the calculated room temperature Gibbs energy $G_{\text{LDA}}(P, 300 \text{ K})$ by setting $G_{\text{corr}}(P, 300 \text{ K}) = G_{\text{LDA}}(P, 300 \text{ K}) + \int_0^P \Delta V(P) dP$. The isotherm derived from $G_{\text{corr}}(P, 300 \text{ K})$ coincides with Dewaele's EOS below 94 GPa, the upper limit of their measurement. Above 200 GPa, $\Delta V(P)$ is almost zero, and the isotherm derived from $G_{\text{corr}}(P, 300 \text{ K})$ is the same as the uncorrected one. The uncertainty due to volume extrapolation in the intermediate region (94 GPa to 200 GPa) is estimated from bulk modulus to be about 1 GPa.

Using $G_{\text{corr}}(P, 300 \text{ K})$ as the base line, we add the computed temperature-dependent part of the Gibbs energy $\Delta G(P, T)$ to $G_{\text{corr}}(P, 300 \text{ K})$, and get the corrected Gibbs energy $G_{\text{corr}}(P, T)$ at temperature T . From $G_{\text{corr}}(P, T)$ we derive all the other thermodynamical properties. Since this correction does not change the temperature dependent part of the Gibbs energy, thermal properties like α , C_P , S , which depend on the temperature derivatives of the Gibbs energy, will not be affected. In contrast, the isothermal bulk modulus K_T and adiabatic bulk modulus K_S will be influenced, as shown in Fig. 9.

After correction, both thermal expansivity and bulk modulus agree with the experiments

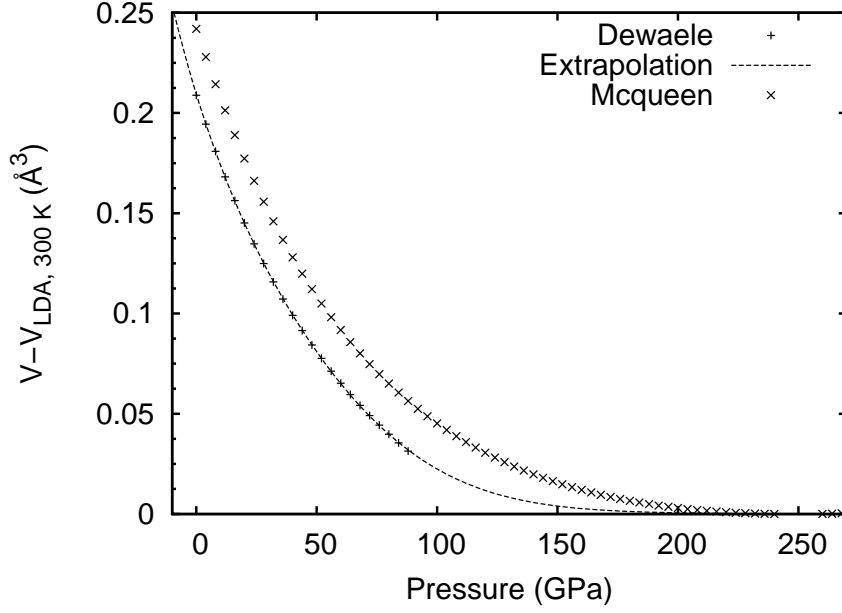


FIG. 8: Volume Correction to the theoretical isotherm at 300 K. Since Dewaele's measurement is within 0-94 GPa, we use $\Delta V(P) = 0.140 \cdot \exp(-P/35.655) + 0.0694 \cdot \exp(-(P/79.01)^2)$ to extrapolate the correction to higher pressure.

well. We expect the product αK_T to be accurate. Integrating αK_T we get the thermal pressure, $P_{th}(V, T) = P(V, T) - P(V, T_0) = \int_{T_0}^T \alpha K_T dT$. The calculated αK_T and P_{th} , before and after correction, are shown in Fig. 10. $P_{th}(V, T)$ is often assumed to be independent of volume and linear in temperature, i.e. αK_T is a constant. Ref. 1 assumes the thermal energy $E(T) = 3k_B T$, the thermal Grüneisen parameter $\gamma = \gamma_0 V/V_0$, where $\gamma_0 = 2.4$, and $V_0 = 15.123 \text{ Å}^3$. The thermal pressure is obtained from Mie-Grüneisen relation

$$P_{th}(V, T) = \frac{E(T)\gamma(V)}{V} = \frac{3k_B \gamma_0}{V_0} \cdot T = 6.57 \times 10^{-3} \cdot T \text{ (GPa)}. \quad (5)$$

In Ref. 4, αK_T is estimated to be $6.94 \times 10^{-3} \text{ GPa/K}$. Both values lie within the variation of the calculated αK_T , as shown in Fig. 10(a). We find that αK_T (P_{th}) has noticeable volume dependence. At fixed temperature, it first decreases, reaches a minimum at about $V/V_0 = 0.8$, then increases. Such behavior originates in the pressure dependence of the thermal expansivity (Fig. 5(b)) and bulk moduli (Fig. 9(b)). This feature has also been observed in Ref. 32, as shown in Fig. 10(b). However it is missing in the previous *ab initio* calculation.⁹

Thermal Grüneisen parameter $\gamma = \frac{\alpha K_T V}{C_V}$ is an important quantity. Empirically it is

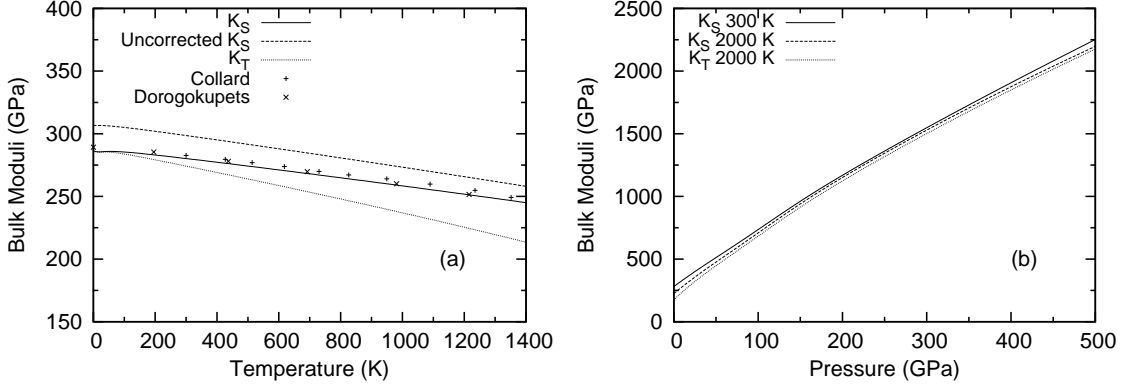


FIG. 9: (a) Bulk moduli at 0 GPa. As noted in Ref. 32, the experimental data in Ref. 41 is inconsistent. The data points we show here are digitized from the graphs in Ref. 41 (denoted as ‘Collard’) and 32 (denoted as ‘Dorogokupets’) respectively. K_S deduced from the corrected Gibbs free energy agrees well with the one computed from empirical models in Ref. 32. (b) Bulk moduli as a function of pressure.

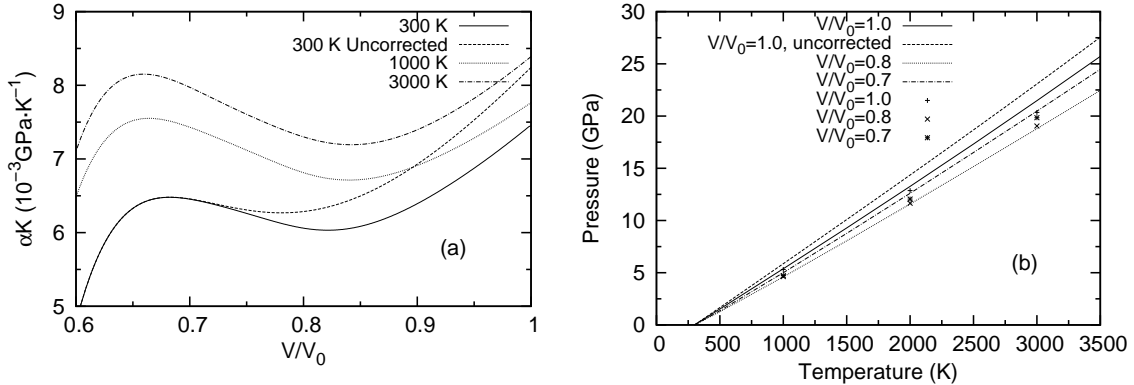


FIG. 10: (a) temperature derivative of P_{th} , $\alpha K_T = \frac{\partial P_{\text{th}}}{\partial T}$ before/after Gibbs energy correction. (b) Thermal pressure P_{th} at different V/V_0 , where V_0 is the experimental volume at ambient condition (15.095 \AA^3). Points are the thermal pressures from Ref. 32.

often assumed to be independent of temperature. Its volume dependence is described by a parameter $q = \frac{\partial \ln \gamma}{\partial \ln V}$, and γ can be represented in q as $\gamma = \gamma_0 \left(\frac{V}{V_0} \right)^q$. From Mie-Grüneisen relation, it is obvious that q is related to the volume dependence of αK_T . If q equals 1, αK_T is independent of volume. If q is greater than 1, αK_T gets smaller as volume decreases. In Ref. 1 q is assumed to equal 1. Fei *et al.*⁸ determined γ by fitting the measured P - V - T data to the Mie-Grüneisen relation up to 27 GPa. They gave $\gamma_0 = 2.72$, $q = 0.5$. Our calculation

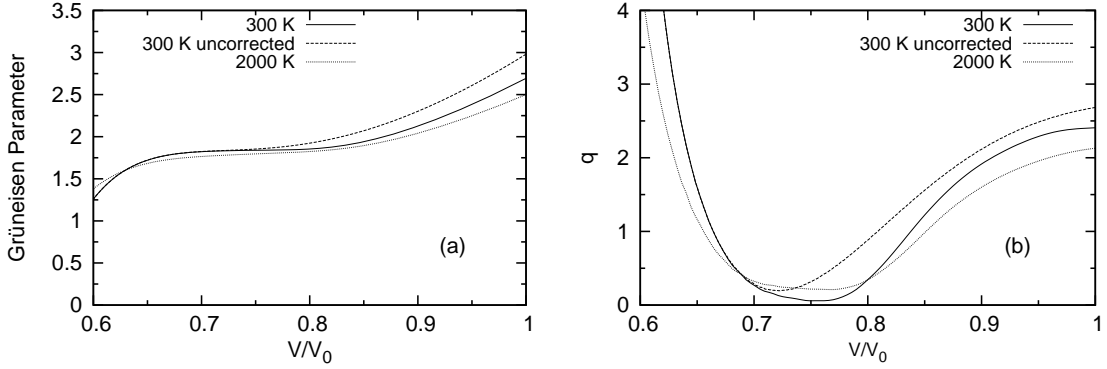


FIG. 11: Thermal Grüneisen parameter (a) volume dependence at fixed temperature; (b) the corresponding q .

indicates the temperature dependence of γ is small. The volume dependence of γ is shown in Fig. 11. The uncorrected DFT calculation tend to overestimate γ . At ambient condition γ_0 equals 2.87. After Gibbs free energy correction, $\gamma_0=2.69$. The corresponding q equals 2.4, much larger than the value obtained in Ref. 8. This is probably due to the small pressure range explored in Ref. 8.

Adding the thermal pressure to the room temperature isotherm, we get the thermal EOS of platinum, as shown in Table III. The existing high temperature P - V - T measurements are only up to 27 GPa and 1873 K. Within this range, the agreement is reasonably good, as shown in Fig. 12. For convenience of interpolation, parametric forms of the thermal EOS are listed in Table IV.

As a final check of our procedure, we start from the corrected Gibbs energy and compute the theoretical Hugoniot by solving the Rankine-Hugoniot equation:

$$E_H(V, T) - E_i(V_0, T_i) = (P_H(V, T) + P_0(V_0, T_i)) \frac{V_0 - V}{2}, \quad (6)$$

where $E_H(V, T)$, $P_H(V, T)$ are the internal energy, pressure at volume V and temperature T . $E_i(V_0, T_i)$, $P_0(V_0, T_i)$ are the internal energy, pressure at the initial volume V_0 and temperature T_i . The results are shown in Fig. 13. The predicted Hugoniot pressure is in good agreement with measurements. The temperature predicted by DFT is lower than the empirically deduced value in Ref. 1. The reduction in Ref. 1 neglects the electronic thermal pressure, and this may cause overestimating Hugoniot temperature.⁴

TABLE III: Pressure (in GPa) as a function of compression ($1-V/V_0$, V_0 is the experimental volume at ambient condition. 15.095 \AA^3) and temperature (in K), deduced from the corrected Gibbs free energy.

| $1 - V/V_0$ | 300 | 500 | 1000 | 1500 | 2000 | 2500 | 3000 | 3500 | 4000 | 4500 | 5000 |
|-------------|--------|--------|--------|--------|--------|--------|--------|--------|--------|--------|--------|
| 0.0 | 0.00 | 1.53 | 5.38 | 9.29 | 13.27 | 17.32 | 21.47 | 25.72 | 30.07 | 34.53 | 39.10 |
| 0.05 | 16.07 | 17.47 | 21.07 | 24.75 | 28.49 | 32.29 | 36.17 | 40.12 | 44.15 | 48.28 | 52.52 |
| 0.10 | 37.83 | 39.14 | 42.55 | 46.04 | 49.60 | 53.21 | 56.88 | 60.61 | 64.41 | 68.29 | 72.27 |
| 0.15 | 67.37 | 68.63 | 71.93 | 75.33 | 78.80 | 82.33 | 85.90 | 89.53 | 93.21 | 96.97 | 100.81 |
| 0.20 | 108.13 | 109.39 | 112.73 | 116.18 | 119.71 | 123.29 | 126.92 | 130.59 | 134.31 | 138.09 | 141.95 |
| 0.25 | 165.76 | 167.07 | 170.56 | 174.17 | 177.85 | 181.58 | 185.36 | 189.19 | 193.05 | 196.97 | 200.94 |
| 0.30 | 247.32 | 248.68 | 252.32 | 256.09 | 259.93 | 263.83 | 267.79 | 271.80 | 275.86 | 279.96 | 284.10 |
| 0.35 | 362.32 | 363.67 | 367.34 | 371.16 | 375.06 | 379.04 | 383.08 | 387.17 | 391.31 | 395.49 | 399.71 |
| 0.40 | 525.87 | 526.94 | 530.04 | 533.36 | 536.80 | 540.30 | 543.84 | 547.40 | 550.99 | 554.62 | 558.31 |

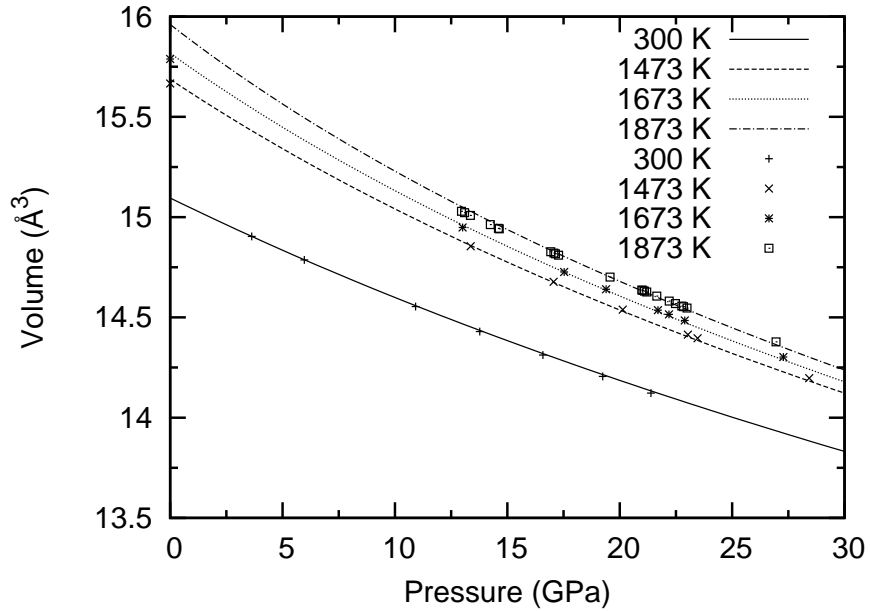


FIG. 12: High temperature isotherms after correcting the Gibbs free energy at 300 K. Lines correspond to the calculated isotherms. The experimental data are taken from Ref. 13, except those at $P=0$ GPa, which are obtained by integrating the thermal expansivity listed in Ref. 37.

TABLE IV: Parametric form of the thermal EOS, $P(V)=P_0 + \frac{3}{2}K_0[(V/V_0)^{-\frac{7}{3}} - (V/V_0)^{-\frac{5}{3}}] \cdot \left\{1 + \frac{3}{4}(K'_0 - 4)[(V/V_0)^{-\frac{2}{3}} - 1] + \frac{3}{8}[K_0K''_0 + (K'_0 - 3)(K'_0 - 4) + \frac{35}{9}][(V/V_0)^{-\frac{2}{3}} - 1]^2\right\}$. At high temperatures, the equilibrium volume may exceed the largest volume we calculate. For better accuracy we fit the P - V - T data in three different pressure-temperature intervals: (1) 0-100 GPa and 0-2000 K, (2) 50-250 GPa and 0-3000 K, (3) 150-550 GPa and 0-5000 K. P_0 denotes the starting pressure of the corresponding interval. V_0 , K_0 , K'_0 , and K''_0 are temperature dependent parameters, and are fitted to a 4th order polynomial $a_0 + a_1t + a_2t^2 + a_3t^3 + a_4t^4$, where $t=T/1000$. They have a formal correspondence to the usual 4th order BM EOS parameters, which are defined at $P_0 = 0$ GPa.

| (1) | a_0 | a_1 | a_2 | a_3 | a_4 |
|--------------------------|-------------|-------------|-------------|--------------|--------------|
| $V_0(\text{\AA}^3)$ | 14.9901 | 0.294003 | 0.202785 | -0.0950538 | 0.0268894 |
| $K_0(\text{GPa})$ | 291.381 | -44.5838 | -10.532 | 5.1353 | -1.52192 |
| K'_0 | 4.69359 | 0.510127 | 0.122011 | -0.0486023 | 0.0355059 |
| $K''_0(\text{GPa}^{-1})$ | -0.0108382 | -0.0081102 | -0.0141626 | 0.00989101 | -0.00469261 |
| (2) | a_0 | a_1 | a_2 | a_3 | a_4 |
| $V_0(\text{\AA}^3)$ | 13.2094 | 0.128576 | 0.0502053 | -0.0160383 | 0.00249748 |
| $K_0(\text{GPa})$ | 504.783 | -29.5221 | -4.01912 | 1.16547 | -0.216303 |
| K'_0 | 5.01683 | 0.197161 | -0.0296035 | 0.0145249 | -0.000659117 |
| $K''_0(\text{GPa}^{-1})$ | -0.0140908 | -0.00339153 | 0.000115756 | -0.000104852 | -3.0538e-05 |
| (3) | a_0 | a_1 | a_2 | a_3 | a_4 |
| $V_0(\text{\AA}^3)$ | 11.4821 | 0.0671833 | 0.0121465 | -0.00243333 | 0.000221517 |
| $K_0(\text{GPa})$ | 969.292 | -21.8351 | -2.99561 | 0.664859 | -0.0675501 |
| K'_0 | 4.12401 | 0.0639489 | -0.00211496 | 0.00237838 | -0.000124486 |
| $K''_0(\text{GPa}^{-1})$ | -0.00446307 | -0.00128202 | 0.00017035 | -6.03469e-05 | 4.09714e-06 |

V. CONCLUSIONS

In this paper, we report our calculations on the static and thermal EOS of platinum using DFT with different exchange correlation functionals. Contrary to previous reports, we find the room temperature isotherm computed with LDA lies below, and nearly parallel

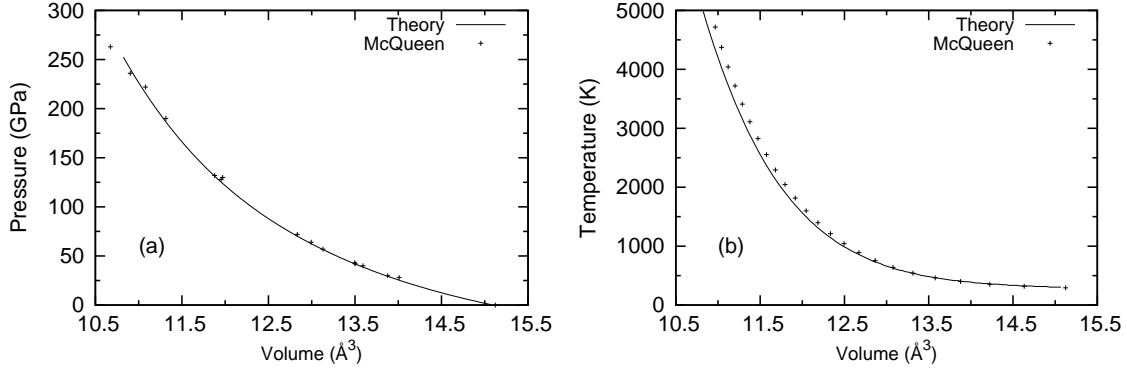


FIG. 13: (a) Theoretical shock Hugoniot compared with the experimental data from McQueen *et al.*(Ref. 1). (b) Temperature along the Hugoniot.

to the experimental compression data. We study the lattice dynamics of platinum within QHA, and find the electronic temperature dependence of vibrations plays a noticeable role in determining the thermal properties of platinum. The calculated thermal properties like α , C_P , $\Delta G(P, T)$ show good agreement to the experimental data, in spite of the fact that anharmonic phonon-phonon interactions and electron-phonon interactions are excluded in our treatment. To provide accurate thermal EOS for pressure calibration, we make corrections to the computed Gibbs energy at room temperature. The resulting thermal EOS seems fairly accurate and we encourage its use as a reference for pressure calibration.

Acknowledgments

We thank P. B. Allen, A. Floris, B. B. Karki for discussions and help. The pseudopotential calculations were performed at the Minnesota Supercomputing Institute (MSI) with the Quantum ESPRESSO package (<http://www.pwscf.org>). The LAPW calculations were performed at Brookhaven National Laboratory (BNL) with the WIEN2k package (<http://www.wien2k.at>). Work by RMW, KU, and ZW was supported by NSF/EAR 0230319, 0635990, and NSF/ITR 0428774 (VLab).

* Electronic address: wentzcov@cems.umn.edu

- ¹ R. G. McQueen, S. P. Marsh, J. W. Taylor, J. M. Fritz, and W. J. Carter, in *High Velocity Impact Phenomena*, edited by R. Kinslow (Academic press, New York, 1970), chap. 7.
- ² J. A. Morgan, *High Temp. High Pressures* **6**, 195 (1974).
- ³ J. C. Jamieson, J. N. Fritz, and M. H. Manghnani, in *High-Pressure Research in Geophysics*, edited by S. Akimoto and M. H. Manghnani (Cent. for Acad. Publ., Tokyo, 1982).
- ⁴ N. C. Holmes, J. A. Moriarty, G. R. Gathers, and W. J. Nellis, *J. Appl. Phys.* **66**, 2962 (1989).
- ⁵ H. K. Mao, Y. Wu, L. C. Chen, and J. F. Shu, *J. Geophys. Res.* **95**, 21737 (1990).
- ⁶ F. D. Stacey and P. M. Davis, *Phys. Earth Planet. Inter.* **142**, 137 (2004).
- ⁷ A. Dewaele, P. Loubeyre, and M. Mezouar, *Phys. Rev. B* **70**, 094112 (2004).
- ⁸ Y. Fei, A. Ricolleau, M. Frank, K. Mibe, G. Shen, and V. Prakapenka, *Proc. Natl. Acad. Sci. USA* **104**, 9182 (2007).
- ⁹ S. Xiang, L. Cai, Y. Bi, F. Jing, and S. Wang, *Phys. Rev. B* **72**, 184102 (2005).
- ¹⁰ E. Menéndez-Proupin and A. K. Singh, *Phys. Rev. B* **76**, 054117 (2007).
- ¹¹ J. P. Perdew and A. Zunger, *Phys. Rev. B* **23**, 5048 (1981).
- ¹² There are two LDA ultrasoft Rappe-Rabe-Kaxiras-Joannopoulos pseudopotentials on the PWSCF (www.pwscf.org) website. ‘Pt.pz-rrkjus.UPF’ is the one without nonlinear core correction ‘Pt.pz-nd-rrkjus.UPF’ includes this correction. Both have a cutoff radius of 2.6 a.u., both yield static EOS stiffer than that of Holmes *et al.* The results reported in PRB (76) 054117 (2007) are very close to our calculations using ‘Pt.pz-nd-rrkjus.UPF’.
- ¹³ Y. Fei, J. Li, K. Hirose, W. Minarik, J. V. Orman, C. Sanloup, W. V. Westrenen, T. Komabayashi, and K. Funakoshi, *Phys. Earth Planet. Inter.* **143-144**, 515 (2004).
- ¹⁴ D. H. Dutton, B. N. Brockhouse, and A. P. Miller, *Can. J. Phys.* **50**, 2915 (1972).
- ¹⁵ P. Blaha, K. Schwarz, G. K. H. Madsen, D. Kvasnicka, and J. Luitz, in *WIEN2k: An Augmented Plane Wave and Local Orbitals Program for Calculating Crystal Properties*, edited by K. Schwarz (Vienna University of Technology, Vienna, Austria, 2001).
- ¹⁶ J. P. Perdew, K. Burke, and M. Ernzerhof, *Phys. Rev. Lett.* **77**, 3865 (1996).
- ¹⁷ Z. Wu and R. E. Cohen, *Phys. Rev. B* **73**, 235116 (2006).
- ¹⁸ H. J. Monkhorst and J. D. Pack, *Phys. Rev. B* **13**, 5188 (1976).
- ¹⁹ P. E. Blöchl, O. Jepsen, and O. K. Andersen, *Phys. Rev. B* **49**, 16223 (1994).
- ²⁰ D. Vanderbilt, *Phys. Rev. B* **41**, 7892 (1990).
- ²¹ S. G. Louie, S. Froyen, and M. L. Cohen, *Phys. Rev. B* **26**, 1738 (1982).

- ²² M. Methfessel and A. T. Paxton, Phys. Rev. B **40**, 3616 (1989).
- ²³ N. D. Mermin, Phys. Rev. **137**, A1441 (1965).
- ²⁴ S. Baroni, P. Giannozzi, and A. Testa, Phys. Rev. Lett. **58**, 1861 (1987).
- ²⁵ S. Baroni, A. D. Corso, S. de Gironcoli, P. Giannozzi, C. Cavazzoni, G. Ballabio, S. Scandolo, G. Chiarotti, P. Focher, A. Pasquarello, et al., URL <http://www.pwscf.org>.
- ²⁶ F. Birch, Phys. Rev. **71**, 809 (1947).
- ²⁷ P. Vinet, J. R. Smith, J. Ferrante, and J. H. Rose, Phys. Rev. B **35**, 1945 (1987).
- ²⁸ R. E. Cohen, O. Gülseren, and R. J. Hemley, Am. Mineral. **85**, 338 (2000).
- ²⁹ T. Tsuchiya and K. Kawamura, Phys. Rev. B **66**, 094115 (2002).
- ³⁰ Y. Wang, R. Ahuja, and B. Johansson, J. Appl. Phys. **92**, 6616 (2002).
- ³¹ C. Bercegeay and S. Bernard, Phys. Rev. B **72**, 214101 (2005).
- ³² P. I. Dorogokupets and A. R. Oganov, Phys. Rev. B **75**, 024115 (2007).
- ³³ A. D. Chijioke, W. J. Nellis, and I. F. Silvera, J. Appl. Phys. **98**, 073526 (2005).
- ³⁴ A. Kavner and R. Jeanloz, J. Appl. Phys. **83**, 7553 (1998).
- ³⁵ This TM pseudopotential is constructed from $5d^9 6s^{0.95} 6p^{0.05}$ atomic configuration, the cutoff radius of $6s$ is 2.6 a.u., which is probably too large. The HGH pseudopotential is constructed from $5s^2 5p^6 5d^{10}$ and does not have this problem.
- ³⁶ A. D. Corso and A. M. Conte, Phys. Rev. B **71**, 115106 (2005).
- ³⁷ R. K. Kirby, Inter. J. of Thermophys. **12**, 679 (1991).
- ³⁸ J. W. Arblaster, Platinum Metals Rev. **38**, 119 (1994).
- ³⁹ R. Maezono, A. Ma, M. D. Towler, and R. J. Needs, Phys. Rev. Lett. **98**, 025701 (2007).
- ⁴⁰ C. W. Greeff and M. J. Graf, Phys. Rev. B **69**, 054107 (2004).
- ⁴¹ S. M. Collard and R. B. McLellan, Acta Metall. Mater. **40**, 699 (1992).